

MODULATED X-RAY EMISSIVITY NEAR THE STRESS EDGE IN SGR A*

MAURIZIO FALANGA^{1,2}, FULVIO MELIA^{3,4}, MARTIN PRESCHER³, GUILLAUME BÉLANGER⁵, ANDREA GOLDWURM^{1,6}

Draft version November 6, 2018

ABSTRACT

Sgr A* is thought to be the radiative manifestation of a $\sim 3.6 \times 10^6 M_{\odot}$ supermassive black hole at the Galactic center. Its mm/sub-mm spectrum and its flare emission at IR and X-ray wavelengths may be produced within the inner ten Schwarzschild radii of a hot, magnetized Keplerian flow. The lightcurve produced in this region may exhibit quasi-periodic variability. We present ray-tracing simulations to determine the general-relativistically modulated X-ray luminosity expected from plasma coupled magnetically to the rest of the disk as it spirals inwards below the innermost stable circular orbit towards the “stress edge” in the case of a Schwarzschild metric. The resulting lightcurve exhibits a modulation similar to that observed during a recent X-ray flare from Sgr A*.

Subject headings: accretion—black hole physics—Galaxy: center—magnetohydrodynamics—plasmas—Instabilities

1. INTRODUCTION

Sgr A*’s time-averaged spectrum is roughly a power law below 100 GHz, with a flux density $S_{\nu} \propto \nu^{\alpha}$, where $\alpha \sim 0.19\text{--}0.34$. In the mm/sub-mm region, however, Sgr A*’s spectrum is dominated by a “bump” (Zylka et al. 1992), indicative of two different emission components (Melia et al. 2000; Agol 2000). Higher frequencies correspond to smaller spatial scales (Melia 1992; Narayan et al. 1995), so the mm/sub-mm radiation is likely produced near the black hole (BH). X-ray flares detected from Sgr A* (Baganoff et al. 2001; Goldwurm et al. 2003; Porquet et al. 2003; Bélanger et al. 2005) may also have been produced within this compact region, either from a sudden increase in accretion accompanied by a reduction in the anomalous viscosity, or from the quick acceleration of electrons near the BH (Liu & Melia 2002; Liu et al. 2004). The energized electrons may also manifest themselves via enhanced emission in a hypothesized jet (Markoff et al. 2001, and references cited therein).

Near-IR flares detected from Sgr A* appear to be modulated with a variable period ≈ 17 minutes (Genzel et al. 2003; Eckart et al. 2006; Meyer et al. 2006; Eckart et al. 2007). The X-ray and near-IR flares may be coupled via the same electron population, so one may expect similarities in their lightcurves. A long X-ray flare detected with XMM-Newton in 2004 also appears to have a modulated lightcurve, though not characterized by a fixed period (Bélanger et al. 2008). If real, the modulation in both the near-IR and X-ray events is almost certainly quasi-periodic rather than periodic, with a decreasing cycle from start to end. But are the fluctuations due to a single azimuthal perturbation (i.e., a “hotspot”),

or from a global pattern of disturbance with a speed not directly associated with the underlying Keplerian period (Tagger & Melia 2006; Falanga et al. 2007)? In this *Letter* we examine the nature of the observed quasi-period, and focus on its implications for the flow of matter through the innermost stable circular orbit (ISCO). A principal result of this study is a ray-tracing simulation of the general-relativistically (GR) modulated lightcurve produced as the disrupted plasma spirals inwards towards the disk’s “stress edge” (Krolik & Hawley 2002).

2. BACKGROUND

Magnetohydrodynamic (MHD) simulations of Sgr A*’s disk demonstrate the growth of a Rossby-wave instability, enhancing the accretion rate for several hours, possibly accounting for the observed flares (Tagger & Melia 2006). The lightcurve produced by GR effects during a Rossby-wave induced spiral pattern in the disk fit the data relatively well, with a quasi-period associated with the pattern speed rather than the Keplerian motion (Falanga et al. 2007). However, MHD simulations of black-hole accretion suggest that magnetic reconnection might take place within the plunging region, due to the presence of a non-axisymmetric spiral density structure, initially caused by the magnetorotational instability (MRI) associated with differential rotation of frozen-in plasma (see, e.g., Hawley 2001).

In this case, the accreting flow is no longer Keplerian because of a radial velocity component. If Sgr A*’s quasi-period of $\sim 17\text{--}25$ minutes is associated with this kind of process rather than a pattern rotation, it would place the corresponding emission region at $0.73\text{--}0.94 r_{\text{ISCO}}$ radii, below the ISCO (where $r_{\text{ISCO}} = 3r_s = 6GM/c^2$) for a Schwarzschild BH. Theoretically, we may therefore distinguish the ISCO from the radius at which the inspiraling material actually detaches from the rest of the magnetized disk—the so-called *stress edge* (Krolik & Hawley 2002). The X-ray modulation would then be associated with the ever-shrinking period of the emitting plasma as it spirals inwards from the magnetic flare.

Interest in “hotspots” began in the early 1980’s in connection with quasi-periodic flux modulations observed in BHs accreting from a binary companion. The hotspots

¹ CEA Saclay, DSM/IRFU/Service d’Astrophysique, 91191 Gif-sur-Yvette, France; mfalanga@cea.fr

² AIM - Unité Mixte de Recherche CEA - CNRS - Université Paris Diderot

³ Physics Department and Steward Observatory, The University of Arizona, Tucson, AZ 85721

⁴ Sir Thomas Lyle Fellow and Miegunyah Fellow

⁵ ESA/ESAC, Apartado 50727, 28080 Madrid, Spain

⁶ UMR Astroparticule et Cosmologie, 10, rue Alice Domont et Léonie Duquet, 75005 Paris Cedex 13, France

are possibly overdense emission regions associated with magnetic instabilities. But even with a hotspot, a Newtonian disk does not produce a modulation since its aspect does not affect the total luminosity observed from it. Other than a dynamical periodicity (such as that due to an azimuthal, radial, or vertical oscillation), only GR effects can produce time-dependent photon trajectories resulting in a modulated lightcurve (see e.g. Cunningham & Bardeen 1973; Abramowicz et al. 1991; Karas & Bao 1992; Hollywood et al. 1995; Falcke et al. 2000; Bromley et al. 2001). Even so, the “standard” disk picture of hotspot modulation has been based on Keplerian motion, for which one then expects a time variability directly related to the Keplerian frequency. Here, the modulation is not associated with such a fixed Keplerian frequency, but from a shrinking orbit and a monotonically decreasing period (see § 3). The relevance of hotspots has already appeared in (Hollywood et al. 1995; Meyer et al. 2006; Eckart et al. 2007; Melia 2007, for review). What is lacking, however, is a non Keplerian treatment of the motion with the intent of probing the stress edge itself.

So where exactly is the inner edge of the accretion disk in Sgr A*? This is a question asked in a broader context by Krolik & Hawley (2002), whose MHD simulations of the plunging region in a pseudo-Newtonian potential identified several characteristic inner radii. Here, we assume a non-spinning BH, so our model pertains solely to the Schwarzschild case.

The monotonic decrease of the period during the flares suggests that we are witnessing the evolution of an event moving inwards across the ISCO. The inflow time scale, t_{inflow} , which determines the rate at which plasma can move from one orbit to another, is given by $\tau_v = r_g/v_{\text{inflow}} \approx 9.6 (r/r_g)^{1/2}$ minutes (Liu & Melia 2002) and is approximately 23.5 minutes at $r = 3r_s = 6r_g$, corresponding to the ISCO for a non-rotating (i.e., $a/r_g = 0$) BH. This time scale does not explicitly depend on a viscosity parameter since the viscosity is directly tied to the MRI physical process via the induced Maxwell stress (Liu & Melia 2002). The inflow time scale defined here characterizes local processes occurring within the innermost portion of the disk during the flares. By comparison, the dynamical time scale, $t_d \approx 1.3 (r/r_g)^{3/2}$, is roughly 19 minutes at this radius (Liu & Melia 2002). Thus, the azimuthal asymmetry giving rise to the modulated flux during the flare may be due to a transient event associated with either a dynamical or viscous process close to the ISCO (Melia et al. 2001).

For a BH mass of $3.6 \times 10^6 M_\odot$, the inflow time scale at $r \approx 2.5 r_s$ (inferred from the *average* period) is just slightly larger than the average period, so the event could be due to the sudden reconfiguration of magnetic field lines frozen into plasma rapidly approaching the ISCO and then flowing across it towards the event horizon. Matter flowing past the ISCO may still remain “magnetically” coupled to the outer accretion flow, so a dynamically more meaningful radius is the so-called *stress edge*, where plunging matter loses dynamical contact with the material farther out (Krolik & Hawley 2002). This may simply be defined as the surface on which the inflow speed first exceeds the magnetosonic speed.

In their simulations, Krolik & Hawley (2002) deter-

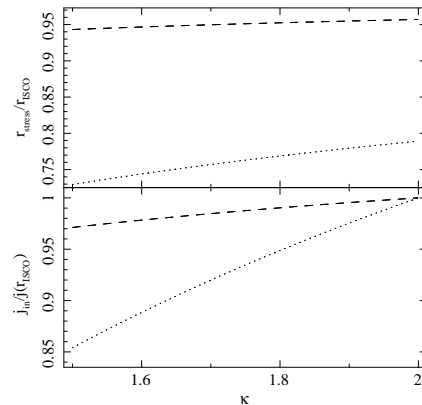


FIG. 1.— Upper panel: The stress edge radius, r_{stress} , in units of r_{ISCO} , as a function of κ , the exponent in the power-law formulation of $\Omega(r)$. The dotted and dashed curves represent a period of 17 and 25 minutes, respectively, using a black-hole mass of $3.6 \times 10^6 M_\odot$ (Schödel et al. 2003). Lower panel: The corresponding ratio of accreted specific angular momentum, j_{in} , to the specific angular momentum at the ISCO.

mined that this surface occurs somewhere between $0.77r_{\text{ISCO}}$ and r_{ISCO} . The specific angular momentum $j = r^2\Omega(r)$, in terms of the orbital angular frequency $\Omega(r)$, continues to fall below r_{ISCO} , though Ω may not necessarily trace its Keplerian value, $\Omega_K(r) \equiv (GM/r^3)^{1/2}$. In the absence of any magnetic coupling across r_{ISCO} , matter would retain all of its specific angular momentum at the ISCO, so that the accreted value of j , which we will call j_{in} , would then simply be $j_{\text{in}} = r_{\text{ISCO}}^2 \Omega_K(r_{\text{ISCO}})$. Instead, the MHD simulations show that $j_{\text{in}} \approx 0.95 j(r_{\text{ISCO}})$, for which r_{stress} is then $\sim 0.8 r_{\text{ISCO}}$, within the range of values indicated by the location of the trans-magnetosonic surface.

If the period in Sgr A* is decreasing monotonically, $j(r)$ will not follow its Keplerian value below r_{ISCO} . Therefore we will adopt the formulation $\Omega(r) = \Omega_0 r^{-\kappa}$ to fit the data in § 3. Clearly, $\kappa = 3/2$ corresponds to Keplerian rotation; κ is 2 in the extreme case of angular momentum conservation. A reasonable fit to the data would therefore be associated with $3/2 \leq \kappa \leq 2$. At the boundary r_{ISCO} , we expect $\Omega = \Omega_K$, which then forces the constant Ω_0 to have the value $c\sqrt{r_g} r_{\text{ISCO}}^{\kappa-3/2}$. We calculate r_{stress} using the quasi-periods 17 and 25 minutes emerging from the X-ray lightcurve (see § 3), and this is plotted as a function of κ in Fig. 1. The radius r_{stress} falls within the range $0.73\text{--}0.96 r_{\text{ISCO}}$ for all permitted values of κ . The corresponding accreted specific angular momentum, for the same parameters as used before (see Fig. 1), is $0.85 j(r_{\text{ISCO}}) \leq j_{\text{in}} \leq j(r_{\text{ISCO}})$ as a function of κ . The ratio $j_{\text{in}}/j(r_{\text{ISCO}}) = 0.95$ from the MHD simulations would require $\kappa \sim 1.8$, for which $r_{\text{stress}} \sim 0.77 r_{\text{ISCO}}$. These results are consistent with the MHD simulations, indicating that the infalling plasma below the ISCO remains magnetically coupled to the outer disk, though the dissipation of angular momentum is not quite strong enough in this region to force the gas into Keplerian rotation.

3. THE INSPIRALING PLASMA MODEL

With $\Omega(r)$ known, we now incorporate strong gravitational effects in a geometrically and optically thin disk, describing the inspiraling disturbance using coordinates (r, θ, φ) in the co-rotating frame. In Fig. 2, we show

the inspiraling trajectory and duration of the emitting plasma. The observer is located at infinity with a viewing angle i relative to the z' -axis in the non-rotating frame, at (observer) polar coordinates (r', θ', φ') . The deflection angle of a photon emitted by plasma in the inspiraling region is ψ , varying periodically with $\cos \psi = \cos i \cos \varphi$, for a disk in the plane $\theta = \pi/2$. Also, for $G = c = 1$, the BH's horizon occurs at $r_s = 2M$, and the last stable orbit is located at $r_{\text{ISCO}} = 3r_s$.

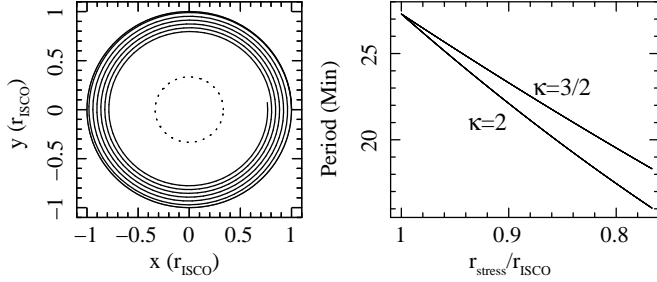


FIG. 2.— Upper panel: The inspiraling trajectory of the hotspot, beginning at r_{ISCO} and terminating at $0.74r_{\text{ISCO}}$. The dotted circle represents the location of the event horizon. Lower panel: The period as a function of the stress radius for the two extreme values of κ adopted here, assuming a black-hole mass of $3.6 \times 10^6 M_{\odot}$.

We calculate the lightcurve using a full ray-tracing algorithm (see Luminet 1979; Falanga et al. 2007). The disk from r_{ISCO} to $90r_s$ is an unperturbed, Keplerian flow, with angular velocity Ω_K , and with specific angular momentum $j_K = r^2 u^\varphi / u^t = r^2 \Omega_K$. The corresponding four-velocity of the effective flow is then $(u^t, u^r, u^\theta, u^\varphi) = u^t(1, 0, 0, \Omega_K)$, where $u^t = (1 - 3M/r)^{-1/2}$ (Misner et al. 1973). The accretion flow is no longer Keplerian below the ISCO.

Triggering a perturbation induces an azimuthal asymmetry in the region $r_{\text{stress}} \approx 0.73 < r < 0.9r_{\text{ISCO}}$. Below r_{ISCO} , we use a simple representation of the bulk velocity field, in which $\Omega(r) = u_{\text{sw}}^\varphi / u_{\text{sw}}^t$, as described e.g., in Fukumura & Tsuruta (2004):

$$v_{\text{sw}}^r = -A_r e^{-(r-r_{\text{stress}})/\Delta_{\text{sw}}} \sin^{\gamma_0} [k_r(r-r_{\text{stress}}) + m\varphi/2 - \varphi_{\text{sw}}/2] \quad (1)$$

In this case, the specific angular momentum is $j_{\text{in}} = r^2 u_{\text{sw}}^\varphi / u_{\text{sw}}^t = \Omega_0 r^{2-\kappa}$. The subscript “sw” denotes the spiral wave, and the number m is the azimuthal wavenumber, fixed to be $m = 1$ for a single-armed spiral wave. The constant $\gamma_0 = 2$ is the width of the spiral wave, $A_r = 0.1$ and $A_\varphi = 0.1$ are the amplitudes chosen to be relatively small, k_r characterizes a tightness (i.e., the number of windings) of the spiral, and the effective radial range of the spiral motion is controlled by $\Delta_{\text{sw}} = 30$, and $\varphi_{\text{sw}} = 0$ denotes the phase of the spiral. Since $(u_{\text{sw}}^r, u_{\text{sw}}^\varphi)$ is not axisymmetric, the net velocity field is also non-axisymmetric. For the effective flow then, $(u_{\text{sw}}^t, u_{\text{sw}}^r, u_{\text{sw}}^\theta, u_{\text{sw}}^\varphi) = u_{\text{sw}}^t(1, v_{\text{sw}}^r, 0, \Omega_0 r^{-\kappa})$, where $u_{\text{sw}}^t = [(1 - 2/m) - (1 - 2m/r)^{-1}(v_{\text{sw}}^r)^2 - r^2 \Omega^2]^{1/2}$, corresponding to the four-vector normalization condition $g_{\alpha\beta} u^\alpha u^\beta = -1$.

We consider four GR effects: (i) light-bending, (ii) gravitational Doppler effect defined as $(1+z)$, taking into

account the non-axisymmetric radial and azimuthal components below r_{ISCO} , (iii) gravitational lensing, $d\Omega_{\text{obs}} = b db d\varphi / D^2$ (with D the distance to the source), expressed through the impact parameter, and (iv) the travel time delay. The relative time delay between photons arriving at the observer from different parts of the disk are calculated from the geodesic equation. The first photon arrives from phase $\varphi = 0$ and $r = r_{\text{ISCO}}$, and defines the reference time, T_0 , which is set to zero. The observed time is then the orbital time plus the light-bending travel time delays, i.e., $T_{\text{obs}}(\varphi_{\text{sw}}, r, i) = \Omega^{-1}(r)\varphi_{\text{sw}} + \Delta T_{\text{GR}}$.

The observed flux at energy E' is $F_{\text{obs}}(E') = I_{\text{obs}}(E') d\Omega_{\text{obs}}$, where $I_{\text{obs}}(E')$ is the radiation intensity observed at infinity and $d\Omega_{\text{obs}}$ is the solid angle on the observer's sky including relativistic effects. Using the relation $I_{\text{obs}}(E', \alpha') = (1+z)^{-3} I_{\text{em}}(E, \alpha)$, a Lorentz invariant quantity that is constant along null geodesics in vacuum, the intensity of a light source integrated over its effective energy range is proportional to the fourth power of the redshift factor, $I_{\text{obs}}(\alpha') = (1+z)^{-4} I_{\text{em}}(r, \varphi)$, $I_{\text{em}}(r, \varphi)$ being the intensity measured in the rest frame of the inspiraling disturbance (Misner et al. 1973). The disk radiates an inverse Compton spectrum, I_{em} , calculated using the parameter scalings, rather than their absolute values. The spectrum parameters are (Melia et al. 2001) the disk temperature, $T(r)$, the electron number density, $n_e(r)$, the magnetic field, $B(r)$, and the disk height $H(r)$. This procedure gives correct amplitudes in the lightcurve, though not the absolute value of the flux per se.

The synchrotron emissivity is therefore $j_s \propto B n_{\text{nt}} \propto B T n_e$, where the nonthermal particle energy is roughly in equipartition with the thermal. The X-rays are produced via inverse Compton scattering from the seed photon number flux. Thus, with $L_{\text{seed}} \propto r^3 j_s$, where j_s is the synchrotron emissivity in units of energy per unit volume per unit time, the soft photon flux scales as the emitted power divided by the characteristic area. That is, $F_{\text{seed}} \propto r^3 j_s / r^2 = r j_s$, which is going to be roughly the same scaling as the seed photon density, so $n_{\text{seed}} \propto r j_s \propto r B T n_e$. The inverse Compton scattering emissivity is therefore $j_{\text{ic}} \propto n_{\text{nt}} n_{\text{seed}} \propto (T n_e)^2 r B$. Thus, $j_x \sim j_{\text{ic}}$, and the surface intensity is $I_{\text{em}} \propto \int j_x ds \propto j_x H$, which gives finally $I_{\text{em}} \propto (T n_e)^2 r B H$.

The flux at a given azimuthal angle φ and radius r is calculated from a numerical computation of $\psi(\alpha)$, followed by a calculation of the Doppler shift, lensing effects, and the flux F_{obs} as a function of the arrival time. For the persistent emission we use the best fit spectral parameters to the *Chandra* data (Melia et al. 2001; Baganoff et al. 2001), described above as a surface emissivity I_{em} . The observed flare normalized flux is modeled with two polynomials, one between 0–100 minutes and the second from 100–160 minutes (see also Meyer et al. 2006). The value k_r is fixed at 11 to have the six observed cycles (see Fig. 3, solid line). The free parameters to fit the data are the inclination angle i and the κ value. The integrated flux is calculated for an extended spiral wave 90° long in the azimuthal direction and $\Delta r = 0.28r_g$ in the radial direction, plus the persistent emission. The MHD simulations show that in the innermost part of the disk a spiral-arm often expands out to $\sim 90^\circ$ (see, e.g., Hawley 2001). The radial extent of the inspiraling region

is set by the observed condition that six cycles should fit within the overall migration of the plasma from the ISCO to the stress edge. In Fig. 3 (solid line), we show the best fit model for $72 \pm 3^\circ$ and $\kappa = 1.7 \pm 0.05$.

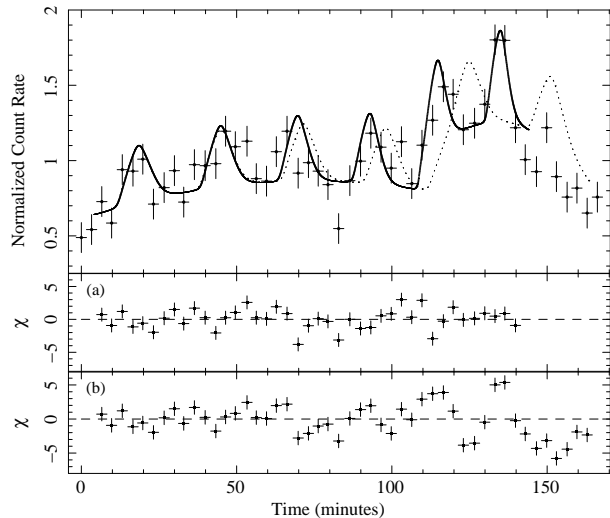


FIG. 3.— Lightcurve of the August 31, 2004 flare in the 2–10 keV energy band (Bélanger et al. 2008), normalized with the observed mean count rate of 0.231 cts s^{-1} for the flare duration. The best fit model for an inspiraling disturbance is shown by the solid line using an inclination angle 72° and $\kappa = 1.7$. The dotted curve represents a constant Keplerian period at the last stable orbit, i.e., r_{ISCO} , $i = 72^\circ$, and $\kappa = 1.5$. Panels (a) and (b) show the residuals (in units of sigma) of the inspiraling and constant-period model, respectively, compared to the data.

4. CONCLUSION

If we adopt the simple view that the last period corresponds to the ISCO, then Sgr A* with a mass of $3.6 \times 10^6 M_\odot$ must be spinning at a rate $a/r_g \gtrsim 0.2 - 0.4$. With a more realistic analysis of the magnetic coupling between matter in the plunging region and that beyond the ISCO, we conclude that the peak of the instability probably occurs at $\sim 0.97 r_{\text{ISCO}}$, where the period is ~ 25 minutes, and the flaring activity continues as the plasma spirals inwards, ending several orbits later when the matter crosses the stress edge at $\sim 0.8 r_{\text{ISCO}}$.

The significance of the fit for an inspiraling disturbance is $\chi^2/d.o.f. = 92.4/39$, compared to $\chi^2/d.o.f. = 285.2/46$ for a fixed Keplerian period (see dotted curve in Figure 3). An inspiraling disturbance is preferred over a fixed orbit by a factor 2.6 in the reduced χ^2 . The residuals in the lower panels of Figure 3 show that the model using a fixed period produces modulations that are progressively shifted in phase with respect to the data, by as much as ~ 16.5 minutes by the end of the flare. The inspiraling model, on the other hand, follows the evolution of the flare and therefore fits the data much better. Plasma on such an orbit also produces a constant pulsed fraction $= (I_{\text{max}} - I_{\text{mean}})/(I_{\text{max}} + I_{\text{min}})$ of $\sim 9\%$, compared with a linear increase from $\sim 9\%$ to $\sim 11\%$ for the inspiraling wave; this effect is due to a radially-dependent gravitational lensing effect. Together, these two effects render the inspiraling scenario a better explanation for the data than the fixed orbit disturbance.

MF is grateful to Keigo Fukumura for helpful discussions. This research was supported by NSF grant AST-0402502 in Arizona, and by the French Space Agency (CNES).

REFERENCES

- Abramowicz, M. A., Bao, G., Lanza, A., Zhang, X.-H., A&A, 245, 454
 Agol, E. 2000, ApJ, 538, L121
 Baganoff, F. et al. 2001, Nature, 413, 45
 Bélanger, G. et al. 2005, ApJ, 635, 1095
 Bélanger, G. et al. 2008, ApJ, submitted (astro-ph/0604337)
 Bromley, B. C., Melia, F., Liu, S. 2001, ApJ Letters, 555, L83
 Cunningham, C. T. & Bardeen, J. 1973, ApJ, 183, 237
 Eckart, A., Schödel, R., Meyer, L. et al. 2006, A&A, 450, 535
 Eckart, A. et al. 2007, A&A, in press, [arXiv:0712.3165]
 Falanga, M. et al. 2007, ApJ, 662, L15
 Falcke, H., Melia, F., Agol, E. 2000, ApJ Letters, 528, L13
 Fukumura, K. & Tsuruta, S. 2004, ApJ, 613, 700
 Genzel, R. et al. 2003, Nature, 425, 934
 Goldwurm, A. et al. 2003, ApJ, 584, 751
 Hawley, J. F., 2001, ApJ, 554, 534
 Hollywood, J. M., Melia, F., Close, L. M. et al., 1995, ApJ, 448, L21
 Karas, V. & Bao, G., 1992, A&A, 257, 531
 Krolik, J. H. & Hawley, J. F. 2002, ApJ, 573, 754
 Liu, S. & Melia, F., 2002, ApJ, 566, L77
 Liu, S., Petrosian, V. & Melia, F. 2004, ApJ, 611, L101
 Lunin, J., -P. 1979, A&A, 75, 228
 Markoff, S., Falcke, H., Yuan, F., Biermann, P. L. 2001, A&A, 379, L13
 Meyer, L., Eckart, A., Schödel, R., et al. 2006, A&A, 460, 15
 Melia, F. 1992, ApJ, 387, L25
 Melia, F. 2007, The Galactic Supermassive Black Hole, PUP (New York)
 Melia, F. Liu, S. & Coker, R. 2000, ApJ, 545, L117
 Melia, F., Liu, S. & Coker, R., 2001, ApJ, 553, 146
 Melia, F., Bromley, B., C., Liu, S., Walker, C., K., 2001, ApJ, 554, L37
 Misner, C. W., Thorne, K., S., & Wheeler, J., A. 1973, *Gravitation* (San Francisco: Freeman)
 Narayan, R., Yi, I. & Mahadevan, R., 1995, Nature, 374, 623
 Porquet, D. et al. 2003, A&A, 407, L17
 Schödel, R., Ott, R., Genzel, R. et al. 2003, ApJ, 596, 1015
 Tagger, M. & Melia, F. 2006, ApJ, 636, L33
 Zylka, R., Mezger, P. & Lesch, H., 1992, A&A, 261, 119